

# RESEARCH PAPER

## Identification of novel macropinocytosis inhibitors using a rational screen of Food and Drug Administration-approved drugs

**Correspondence** Gábor Csányi, Vascular Biology Center, Augusta University, Augusta, GA, USA. E-mail: gcsanyi@augusta.edu

**Received** 8 January 2018; **Revised** 8 May 2018; **Accepted** 13 June 2018

Hui-Ping Lin<sup>1</sup> , Bhupesh Singla<sup>1</sup>, Pushpankur Ghoshal<sup>1</sup>, Jessica L Faulkner<sup>1</sup>, Mary Cherian-Shaw<sup>1</sup>, Paul M O'Connor<sup>2</sup>, Jin-Xiong She<sup>3</sup>, Eric J Belin de Chantemele<sup>1</sup> and Gábor Csányi<sup>1,4</sup>

<sup>1</sup>Vascular Biology Center, Augusta University, Augusta, GA, USA, <sup>2</sup>Department of Physiology, Augusta University, Augusta, GA, USA, <sup>3</sup>Center for Biotechnology and Genomic Medicine, Augusta University, Augusta, GA, USA, and <sup>4</sup>Department of Pharmacology and Toxicology, Augusta University, Augusta, GA, USA

### BACKGROUND AND PURPOSE

Macropinocytosis is involved in many pathologies, including cardiovascular disorders, cancer, allergic diseases, viral and bacterial infections. Unfortunately, the currently available pharmacological inhibitors of macropinocytosis interrupt other endocytic processes and have non-specific endocytosis-independent effects. Here we have sought to identify new, clinically relevant inhibitors of macropinocytosis, using an FDA-approved drug library.

### EXPERIMENTAL APPROACH

In the present study, 640 FDA-approved compounds were tested for their ability to inhibit macropinocytosis. A series of secondary assays were performed to confirm inhibitory activity, determine IC<sub>50</sub> values and investigate cell toxicity. The ability of identified hits to inhibit phagocytosis and clathrin-mediated and caveolin-mediated endocytosis was also investigated. Scanning electron microscopy and molecular biology techniques were utilized to examine the mechanisms by which selected compounds inhibit macropinocytosis.

### KEY RESULTS

The primary screen identified 14 compounds that at ~10 µM concentration inhibit >95% of macropinocytotic solute internalization. Three compounds - imipramine, phenoxybenzamine and vinblastine - potently inhibited (IC<sub>50</sub> ≤ 131 nM) macropinocytosis without exerting cytotoxic effects or inhibiting other endocytic pathways. Scanning electron microscopy imaging indicated that imipramine inhibits membrane ruffle formation, a critical early step leading to initiation of macropinocytosis. Finally, imipramine has been shown to inhibit macropinocytosis in several cell types, including cancer cells, dendritic cells and macrophages.

### CONCLUSIONS AND IMPLICATIONS

Our results identify imipramine as a new pharmacological tool to study macropinocytosis in cellular and biological systems. This study also suggests that imipramine could be a good candidate for repurposing as a therapeutic agent in pathological processes involving macropinocytosis.

### Abbreviations

BCECF-AM, 2',7'-bis-(2-carboxyethyl)-5-(and-6)-carboxyfluorescein-acetoxymethyl; EIPA, 5-(N-ethyl-N-isopropyl)amiloride; FDA, Food and Drug Administration; M-CSF, macrophage colony-stimulating factor; MEK, MAPK kinase; NHE, sodium/hydrogen exchanger; nLDL, native LDL; PMA, phorbol 12-myristate 13-acetate

## Introduction

Endocytic membrane trafficking plays an essential role in delivering membrane components, receptor-associated ligands, extracellular fluid and pericellular solute molecules inside the cell. Three major categories of endocytic processes have been described: phagocytosis, receptor-mediated endocytosis and pinocytosis (Bohdanowicz and Grinstein, 2013). These internalization processes can be distinguished by the size of the vesicle formed, the physical characteristics of the cargo and the endocytic machineries involved. Macropinocytosis (also known as fluid-phase endocytosis or cell drinking) is distinct in many ways from the better characterized receptor-mediated endocytosis and phagocytosis. Macropinocytotic internalization of pericellular solutes does not require physical interaction with the plasma membrane (i.e. receptor binding), while phagocytosis and receptor-mediated endocytosis are ligand–receptor-driven processes (Mercer and Helenius, 2009). Phagocytosis (solid-phase endocytosis or cell eating) requires localized and transient remodelling of actin filaments, resulting in a coherent growth of the plasma membrane around the particle, formation of the phagosome and particle internalization (Botelho *et al.*, 2000). Receptor-mediated endocytosis is largely an actin-independent process stimulated by specific cell-surface receptors, such as **C-type lectin receptors**, Fcγ and Fcε and subsequent translocation of adaptor proteins to the plasma membrane (Berry and Call, 2017). In contrast to phagocytosis and receptor-mediated endocytosis, macropinocytosis is initiated by extensive, submembranous activation of the actin cytoskeleton resulting in plasma membrane ruffling over the entire dorsal surface of the cell or the cellular periphery (Grimmer *et al.*, 2002; Bohdanowicz and Grinstein, 2013). Membrane ruffles adhere to the non-extended plasma membrane or circularize, fuse on the lateral side and close, resulting in a massive internalization of extracellular fluid (up to 40% of the cell volume  $\text{h}^{-1}$ ; Sallusto *et al.*, 1995; Norbury, 2006) and associated solutes into heterogeneous vacuoles (0.2–5  $\mu\text{m}$ ), called macropinosomes (Chung *et al.*, 2015).

Macropinocytosis can be induced in many cell types upon stimulation with phorbol esters, cytokines and growth factors (Nakase *et al.*, 2015; Ghoshal *et al.*, 2017). Consistent with this statement, an increased rate of solute macropinocytosis has been shown to facilitate phenotypic and functional changes in a wide variety of cell types and contribute to the development of various pathological processes. For instance, internalization of extracellular proteins through macropinocytosis is utilized by cancer cells to support their unique metabolic needs, leading to increased cancer cell proliferation *in vitro* and tumour growth *in vivo* (Comisso *et al.*, 2013). Vaccinia, adeno, picorna and other virus families and several types of bacteria, including *Shigella*, *Mycobacterium*, *Salmonella* and *Legionella*, ‘learn’ how to stimulate membrane ruffling and invade host cells *via* macropinocytosis (Mercer and Helenius, 2009; Lim and Gleeson, 2011). Renal tubular cells internalize calcium oxalate monohydrate crystals *via* macropinocytosis, a process that may contribute to nephrolithiasis (Kanlaya *et al.*, 2013). Macropinocytosis of amyloid precursor protein in neuronal cells has been implicated in the pathogenesis of Alzheimer’s disease (Tang *et al.*, 2015). Evidence has also been

accumulating that macrophages internalize exogenous lipids *via* macropinocytosis, leading to foam cell formation, a key pathological event in the initiation and progression of atherosclerosis (Kruth *et al.*, 2005; Csanyi *et al.*, 2017). Despite this information, no clinically useful inhibitors of macropinocytosis are available to inhibit macropinocytosis in pathological processes.

The currently available pharmacological tools to inhibit macropinocytosis are limited and comprise (i) actin polymerization inhibitors (Aleksandrowicz *et al.*, 2011), (ii) **PI3K** blockers (Araki *et al.*, 1996) and (iii) inhibitors of **sodium/hydrogen exchangers (NHEs)** (Koivusalo *et al.*, 2010). The actin perturbant cytochalasin D and latrunculins have been shown to inhibit membrane ruffling and macropinocytosis. However, they also block phagocytosis and all other cellular processes involving actin polymerization (Stockinger *et al.*, 2006). The PI3K inhibitor **wortmannin** and LY290042 block macropinocytosis and phagocytosis in macrophages, fibroblasts and epithelial cells (Ivanov, 2008). As PI3K is an upstream mediator of **Akt**, **mTOR** and **NOS** and known to regulate signalling processes downstream of glucose and amino acid uptake (Kohn *et al.*, 1996), wortmannin and LY290042 are expected to inhibit many cellular processes in addition to macropinocytosis. The **epithelial sodium channel** blocker **amiloride** inhibits both constitutive and stimulated macropinocytosis and also phagocytosis in a variety of mammalian cells (Ivanov, 2008; Zhang *et al.*, 2015). Currently, the selective NHE blocker **ethyl-isopropyl amiloride (EIPA)** and dimethyl amiloride are considered to be the first choices for pharmacological inhibition of macropinocytosis (Ivanov, 2008). However, possible endocytosis-unrelated effects of these drugs on ion transport, intracellular pH and cytoskeleton limit their use as pharmacological inhibitors of macropinocytosis.

Considering these limitations in the field of endocytosis, the goal of the present study was to perform a systematic screen of a wide range of FDA-approved drugs to identify new, clinically relevant inhibitors of macropinocytosis. One of the most effective strategies for drug development is the repurposing of existing drugs that have been approved by the FDA for human therapy (Ashburn and Thor, 2004). The key advantage of drug repurposing is that the drugs have already undergone extensive safety and bioavailability testing and thus allow more rapid clinical development at a lower cost compared with *de novo* drug development. FDA-approved drug libraries provide rich sources of bioactive agents that have been carefully selected to maximize chemical and pharmacological diversity. In the present study, we first optimized a cell-based macropinocytosis assay for screening purposes. Following optimization, 640 FDA-approved compounds were tested for their ability to inhibit macropinocytosis. The primary screen identified 14 compounds that at ~10  $\mu\text{M}$  concentration inhibit >95% of macropinocytotic solute internalization. A series of secondary assays were performed to confirm inhibitory activity, determine  $\text{IC}_{50}$  values and investigate cell toxicity. To investigate selectivity, we tested whether the candidate compounds inhibit phagocytosis, caveolae-dependent endocytosis and clathrin-mediated endocytosis. We identified one compound that potentially ( $\text{IC}_{50}$  = 131 nM) inhibit macropinocytosis,

without exerting cytotoxic effects or inhibiting other endocytic pathways. Finally, the ability of the identified compound to inhibit macropinocytosis in several cell types, including cancer cells, dendritic cells and macrophages, was confirmed.

## Methods

### Animals

All animal care and experimental procedures were approved by the Institutional Animal Care and Use Committee (IACUC), Augusta University, Augusta, USA. Animal studies are reported in compliance with the ARRIVE guidelines (Kilkenny *et al.*, 2010; McGrath and Lilley, 2015). Every effort was made to minimize animal suffering and to reduce the number of animals used. Eight- to ten-week-old male, C57BL/6 mice were purchased from The Jackson Laboratory (Bar Harbor, ME, USA). Mice were housed at controlled temperatures (21–23°C) with *ad libitum* access to standard rodent chow and water and 12 h light–dark cycles. Mice were anaesthetized (isoflurane inhalation, 3%) and killed by cervical dislocation and exsanguinated. The mice were non-blindly randomized prior to tissue isolation.

### Cell culture

RAW 264.7 macrophages (ATCC, Manassas, VA, USA) and 4T1 cells [ATCC; provided by Dr Ali Arbab (Augusta University)] were maintained in DMEM (Mediatech, Inc., Manassas, VA, USA) supplemented with 100 IU·mL<sup>-1</sup> of penicillin G, 100 µg·mL<sup>-1</sup> streptomycin and 10% (vol/vol) heat-inactivated FBS in a humidified incubator at 37°C and 5% CO<sub>2</sub>. Bone marrow-derived monocytes were cultured in RPMI-1640 medium containing 100 IU·mL<sup>-1</sup> of penicillin G, 100 µg·mL<sup>-1</sup> streptomycin and 10% FBS. Monocytes were differentiated into macrophages using murine macrophage colony-stimulating factor (M-CSF; 20 ng·mL<sup>-1</sup>, 6 days) or dendritic cells using GM-CSF (20 ng·mL<sup>-1</sup>, 6 days) and IL-4 (2 ng·mL<sup>-1</sup>, 6 days) as previously described (Thomas and Lipsky, 1996; Potts *et al.*, 2008).

### Flow cytometry

Flow cytometry experiments were performed using the Becton Dickinson (Franklin Lakes, NJ, USA) FACSCalibur flow cytometer using a standard protocol (Ghoshal *et al.*, 2017).

**Design of screen.** RAW 264.7 macrophages were plated in 24-well plates at a density of  $1 \times 10^6$  cells mL<sup>-1</sup>. Twenty-four hours later, macrophages were pre-incubated with vehicle, candidate drugs (1–10 µM) or EIPA (positive control; 25 µM) for 60 min, treated with FITC-dextran (70 000 MW, 150 µg·mL<sup>-1</sup>) and macropinocytosis stimulated using PMA (1 µM; 2 h). Cells were fixed in 2% PFA, resuspended in FACS buffer (2% BSA and 0.01% sodium azide in PBS) and stained with the LIVE/DEAD™ Fixable Far Red dye to identify live cells. Fluorescence intensity was measured using the FL1 channel for FITC (Ex: 488 nm; Em: 530 nm) and FL4 channel for LIVE/DEAD™ Fixable Far Red dye (Ex: 650 nm; Em: 660 nm). Representative FACS experiments are shown in Figure 1B.

**Foam cell formation.** RAW 264.7 macrophages were treated with vehicle, **PMA** (1 µM) or **imipramine** (5 µM; 1 h pre-incubation) + PMA in the presence of nLDL (250 µg·mL<sup>-1</sup>) for 24 h. Cells were fixed in 2% PFA and stained with Nile Red (25 ng·mL<sup>-1</sup>) for 10 min. Fluorescence intensity was measured using the FL3 channel for Nile Red (Ex: 488 nm; Em: 670 nm).

**Cancer cell macropinocytosis.** 4T1 mammary carcinoma cells were pre-incubated with imipramine (5 µM) for 1 h and treated with vehicle or PMA (1 µM) in the presence of FITC-dextran (70 000 MW, 150 µg·mL<sup>-1</sup>) for 2 h. Fluorescence intensity was measured using the FL1 channel for FITC (Ex: 488 nm; Em: 530 nm).

**Dendritic cell macropinocytosis.** Bone marrow-derived **CD11c**-positive dendritic cells were pretreated with imipramine (5 µM, 1 h), incubated with FITC-ovalbumin (70 000 MW, 150 µg·mL<sup>-1</sup>) and treated with vehicle or PMA (1 µM) for 2 h. Fluorescence intensity was measured using the FL1 channel for FITC (Ex: 488 nm; Em: 530 nm).

**Clathrin-mediated and caveolin-mediated endocytosis.** Receptor-mediated uptake of FITC-transferrin (1 µg·mL<sup>-1</sup>; clathrin-mediated endocytosis) and Alexa Fluor 488-albumin (1 µg·mL<sup>-1</sup>; caveolin-mediated endocytosis) was investigated in RAW 264.7 macrophages following their incubation with vehicle (negative control), candidate drugs (IC<sub>100</sub> concentration, 1 h) or positive controls for clathrin-mediated (**chlorpromazine**, 10 µM, 1 h) and caveolin-mediated endocytosis (nystatin, 10 µM, 1 h). Fluorescence intensity was measured using the FL1 channel for FITC and Alexa Fluor 488 (Ex: 488 nm; Em: 530 nm).

### Phagocytosis assay

Phagocytosis was investigated using the CytoSelect™ 96-Well Phagocytosis Assay Kit (Cell Biolabs, San Diego, CA, USA) according to the manufacturer's instructions. Briefly, RAW 264.7 macrophages were plated in 96-well plates at a density of  $0.5 \times 10^6$  cells mL<sup>-1</sup>. Cells were pretreated with vehicle (negative control), selected macropinocytosis inhibitors (IC<sub>100</sub> concentration, 1 h) and cytochalasin D (2 µM, 1 h) and then incubated with enzyme-labelled, *Escherichia coli* particles (10 µL per well) for 6 h. Adherent cells were fixed with 3.2% buffered formaldehyde solution and blocked for 30 min at room temperature on an orbital shaker. After permeabilization, the substrate solution was added, and the mixture was incubated for 30 min at room temperature. The reaction was stopped, and absorbance was read at 450 nm using a Clariostar Monochromator Microplate Reader (BMG Labtech, Cary, NC, USA).

### Cytotoxicity assay

Cytotoxicity was investigated using the Thermo Fisher LDH Cytotoxicity Assay Kit according to the manufacturer's instructions.

### Imaging experiments

**Confocal microscopy.** Following treatment, macrophages were fixed in 2% PFA, permeabilized with 0.1% Triton X-100 and stained with Alexa Fluor 488® phalloidin and

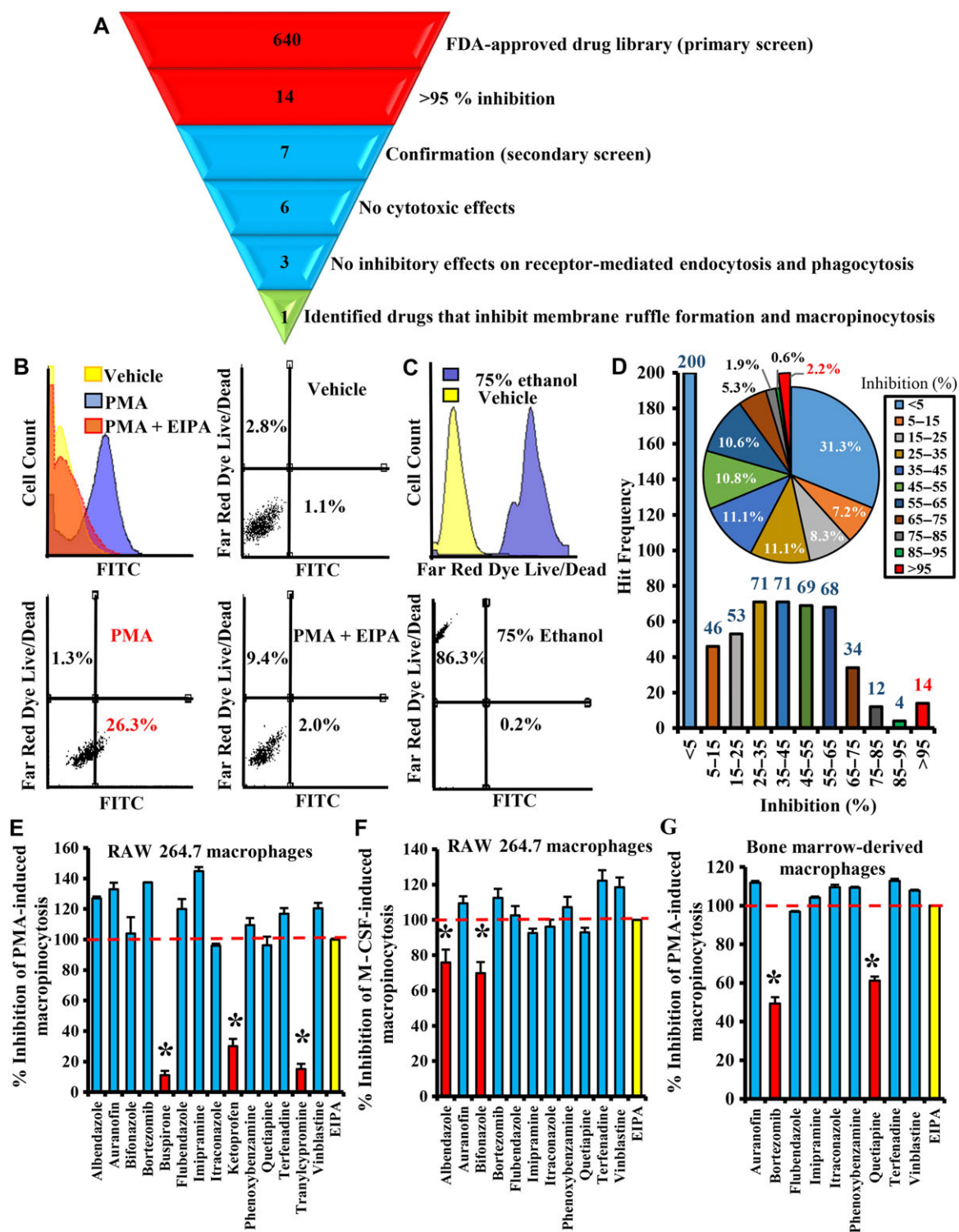


Figure 1

Identification of new macropinocytosis inhibitors from a library of FDA-approved drugs using primary and secondary screens. (A) Schematic representation of the screening strategy. Results from primary screen are red, follow-up screens are in blue and identified macropinocytosis inhibitors are shown in green. (B) Representative flow cytometry data illustrating FITC-dextran macropinocytosis in RAW 264.7 macrophages. (C) Live cell gating strategy. (D) Summary of the primary screen. Secondary confirmatory screens validating the ability of hits from the primary screen to inhibit (E) PMA-induced and (F) M-CSF-induced FITC-dextran macropinocytosis in RAW 264.7 macrophages ( $n = 5$ ). (G) Inhibitory activity of identified compounds in primary murine macrophages ( $n = 5$ ). Data were expressed as % of EIPA-induced inhibition of FITC-dextran uptake. Data represent the mean  $\pm$  SEM. \* $P < 0.05$ , significantly different from EIPA control by one-way ANOVA with Bonferroni *post hoc* test.



Hoechst 33342 (ThermoFisher, Grand Island, NY, USA). Images were captured using a Zeiss (San Diego, CA, USA) 780 inverted confocal microscope.

**Scanning electron microscopy.** Macrophages were fixed (4% PFA, 2% glutaraldehyde in 0.1 M sodium cacodylate solution) overnight at 4°C. Then the cells were dehydrated through a graded ethanol series (25–100%) and washed with 100% ethanol before critical point drying (Tousimis Samdri-790; Tousimis, Rockville, MD, USA). Coverslips were mounted onto aluminium stubs and sputter coated with 3.5 nm of gold/palladium (Anatek USA-Hummer, Union City, CA, USA). Cells were imaged at 20 kV using a Philips XL30 scanning electron microscope (FEI, Hillsboro, OR, USA).

### Determination of NHE-1 activity

Activity of NHE was determined as described previously using the dual-excitation ratiometric pH indicator, acetoxymethyl ester of 29,79-bis(carboxyethyl)-5(6)-carboxyfluorescein (BCECF-AM) (Molecular Probes, Inc., Eugene, OR, USA) (Swanson *et al.*, 1998). Briefly, RAW 264.7 macrophages were grown on glass coverslips in DMEM with 10% FBS and growth arrested at 70–80% confluence by incubation in DMEM with 1% FBS for 24 h. Cells were pre-incubated with vehicle, EIPA (positive control; 25  $\mu$ M) or imipramine (5  $\mu$ M) for 60 min and then loaded with BCECF-AM (3 mM) for 30 min. Cells were washed twice and incubated in a HEPES-Tris balanced salt solution (130 mM NaCl, 5 mM KCl, 1.5 mM CaCl<sub>2</sub>, 1.0 mM MgCl<sub>2</sub> and 20 mM HEPES; pH 7.4) for 30 min. All subsequent experiments were performed at 25°C. Cells were acid loaded by incubation with HEPES-Tris-buffered salt solution containing 20 mM NH<sub>4</sub>Cl, followed by washing with HEPES-Tris-buffered salt solution without NH<sub>4</sub>Cl. Removal of NH<sub>4</sub>Cl is followed by cytosolic acidification due to NH<sub>3</sub> exit with cytosolic dissociation of NH<sub>4</sub><sup>+</sup> and retention of H<sup>+</sup>. The rate of pH recovery from acidosis was recorded over the next 10 min. The pH-dependent fluorescent signal of BCECF-AM was obtained by illuminating the samples at excitation wavelengths of 490 and 440 nm using a Nikon (Melville, NY, USA) TE2000 inverted microscope. The ratio of signals obtained at 490 and 440 nm wavelengths was used to monitor changes in intracellular pH. The contribution of NHE to pH recovery was confirmed by treatment with EIPA.

### Western blot

Western blotting was performed as previously described using the Odyssey CLx Infrared Imaging System (Li-Cor Biosciences, Lincoln, NE, USA) (Csanyi *et al.*, 2012). Briefly, protein concentration was estimated using the bicinchoninic acid protein assay (Pierce Biotechnology, Rockford, IL, USA), according to manufacturer's instructions. Equal amounts of protein (30  $\mu$ g) were heated in Laemmli sample buffer (Bio-Rad Laboratories, Inc., Hercules, CA, USA) at 95°C for 5 min, separated on SDS-PAGE gels, transferred onto nitrocellulose membranes (Li-Cor Biosciences) and probed with the following primary antibodies: **MEK**, p-MEK, **ERK**, p-ERK, **PKC $\delta$** , p-PKC $\delta$  and  $\beta$ -tubulin (Cell Signaling, Danvers, MA, USA; rabbit, 1:1000). The IRDye-conjugated secondary antibodies (Li-Cor Biosciences) were used to detect the primary antibodies.

### PI3K activity

PI3K activity was measured using the Echelon's PI3-Kinase Activity ELISA: Pico kit (Echelon Biosciences).

### ROS measurement

L-012, a luminol-based chemiluminescent probe, was used to determine O<sub>2</sub><sup>-</sup> generation as described previously (Ghoshal *et al.*, 2017). RAW 264.7 macrophages (5  $\times$  10<sup>4</sup> cells per well) were plated in white flat bottom 96-well microplates in sterile PBS containing L-012 (400  $\mu$ M; Wako Chemicals) in the presence and absence of PMA (1  $\mu$ M) and imipramine (5  $\mu$ M). The chemiluminescence signal was measured every 2 min for 2 h at 37°C using a Clariostar Monochromator Microplate Reader (BMG Labtech). The specificity of L-012 for O<sub>2</sub><sup>-</sup> was confirmed by the addition of SOD (150 U·mL<sup>-1</sup>).

### Data and statistical analysis

The data and statistical analysis comply with the recommendations on experimental design and analysis in pharmacology (Curtis *et al.*, 2018). All data are expressed as means  $\pm$  SEM. Statistical analysis was performed using GraphPad Prism 7 (La Jolla, CA, USA). One-way ANOVA, followed by a Bonferroni *post hoc* test, was used to analyse statistical differences. A *P*-value less than 0.05 was considered statistically significant.

### Materials

PMA, Nile Red, EIPA, bortezomib, flubendazole, **terfenadine**, **quetiapine** hemifumarate, itraconazole, **phenoxybenzamine**, **vinblastine**, albendazole, **auranofin**, imipramine, bifenazone, **bupirone**, **ketopromazine**, **tranlycypromine**, chlorpromazine, nystatin and FITC-dextran were purchased from Sigma-Aldrich (St. Louis, MO, USA). Human nLDL was obtained from Kalen Biomedical, LLC (Montgomery Village, MD, USA). M-CSF was purchased from Miltenyi Biotec Inc. (San Diego, CA, USA). LDH Cytotoxicity Assay Kit, LIVE/DEAD™ Fixable Far Red Dead Cell Stain Kit and FITC-ovalbumin were obtained from Thermo Fisher Scientific (Grand Island, NY, USA). SCREEN-WELL® FDA-approved drug library V2 (Product #: BML-2841-0100) was obtained from Enzo Life Sciences (Farmingdale, NY, USA). PI3-Kinase Activity ELISA: Pico kit was obtained from Echelon Biosciences (Salt Lake City, UT, USA). L-012 was obtained from Wako Chemicals (Richmond, VA, USA).

### Nomenclature of targets and ligands

Key protein targets and ligands in this article are hyperlinked to corresponding entries in <http://www.guidetopharmacology.org>, the common portal for data from the IUPHAR/BPS Guide to PHARMACOLOGY (Harding *et al.*, 2018), and are permanently archived in the Concise Guide to PHARMACOLOGY 2017/18 (Alexander *et al.*, 2017a,b,c,d,e).

## Results

### Primary and secondary screens

In order to identify chemical compounds that inhibit macropinocytosis, we performed a systemic screen of the

Screen-Well™ FDA Approved Drug Library (Enzo Life Sciences), which contains 640 structurally and pharmacologically diverse FDA-approved drugs. An acceptable inhibitor would inhibit macropinocytosis at low concentrations but lack inhibitory activity against phagocytosis and receptor-mediated endocytosis. Schematic representation of the screening strategy to identify such compounds is shown in Figure 1A. Accordingly, we first optimized a cell-based assay using RAW 264.7 macrophages incubated with FITC-dextran (70 000 MW, 150  $\mu\text{g}\cdot\text{mL}^{-1}$ ) and **PMA** (1  $\mu\text{M}$ ; macropinocytosis stimulator), with or without EIPA (25  $\mu\text{M}$ ; macropinocytosis inhibitor) as a detection system for macropinocytosis (Figure 1B). FITC-dextran macropinocytosis was quantified in live cells identified by the Live/Dead™ Fixable Far Red dye (Figure 1B, C). Following optimization, a primary screen using a 1–10  $\mu\text{M}$  final compound concentration to identify compounds capable of inhibiting macropinocytosis was performed. In each plate, row 1, column 1 contained no compounds and no FITC-dextran; row 1, column 2 contained only FITC-dextran; row 1, column 3 contained FITC-dextran and PMA; and row 1, column 4 contained FITC-dextran, EIPA (60 min pre-incubation) and PMA. FDA-approved compounds were administered in row 1 through 4. Finally, each plate contained a second set of controls in row 4. The primary screen led to the identification of 14 compounds (hit rate: 2.2%) that inhibit PMA-induced FITC-dextran internalization by more than 95% in RAW 264.7 macrophages (Figure 1D). Next, a series of secondary experiments were performed to confirm inhibitory activities of identified compounds. Eleven out of 14 drugs (78%) were confirmed to inhibit FITC-dextran internalization (>95%) in response to PMA treatment in RAW 264.7 cells (Figure 1E). Of these hits, two compounds were excluded due to incomplete (~70%) inhibition in response to the physiological macropinocytosis stimulator, macrophage colony-stimulating factor (M-CSF) (Yoshida *et al.*, 2009; Ghoshal *et al.*, 2017) (Figure 1F). Two additional compounds were eliminated from further analysis due to their incomplete inhibition of macropinocytosis in primary mouse macrophages (Figure 1G). The primary screen of the library and subsequent secondary analyses identified seven compounds that inhibit stimulated macropinocytosis at low micromolar concentrations in macrophages.

### Determination of $\text{IC}_{50}$ values

Individual serial dilutions of the seven lead compounds (flubendazole, terfenadine, itraconazole, phenoxybenzamine, vinblastine, auranofin and imipramine) at concentrations ranging from 0 to 50  $\mu\text{M}$  (5 $\times$ ) were prepared and incubated with RAW cells (60 min), followed by treatment with FITC-dextran and stimulation with PMA.  $\text{IC}_{50}$  values were calculated from logarithmic scale plots of the inhibitor concentrations against the percentage of inhibitory activity relative to the uninhibited control, using Prism software (GraphPad Software Inc., San Diego, CA, USA). The  $\text{IC}_{50}$  values for flubendazole, terfenadine, itraconazole, phenoxybenzamine, vinblastine, auranofin and imipramine are shown in Figure 2A–G and Table 1. For all subsequent experiments, the maximal inhibitory concentration ( $\text{IC}_{100}$ ) of identified compounds was used (Table 1).

### Cytotoxicity and selectivity

An undesirable side effect would be the reduction of solute internalization in the assays due to cell death following longer drug exposure rather than a direct inhibition of macropinocytosis. To verify that this was not the case for the identified compounds, the 50% cytotoxic concentration ( $\text{CC}_{50}$ ) values of identified inhibitors were determined using a commercially available LDH cytotoxicity kit (Thermo Fisher). This assay quantitatively measures LDH released into the media due to compromised plasma membrane integrity (i.e. dead cells). The  $\text{CC}_{50}$  values were calculated from logarithmic scale plots of the inhibitor concentrations against the percentage of cytotoxic activity, using Prism software (Table 1). The calculated selectivity indexes ( $\text{SI} = \text{CC}_{50}/\text{IC}_{50}$ ) are shown in Table 1. As shown in Figure 3A, flubendazole treatment (9  $\mu\text{M}$ , 24 h) induced LDH release (~31.5% of the positive control, lysis solution) following a longer exposure. Due to its lower selectivity index ( $\text{SI} = 14.2$ ), flubendazole was excluded from further analysis.

As mentioned, an acceptable macropinocytosis inhibitor would not only block macropinocytosis but also should be inactive against other endocytic processes. Of the six remaining compounds, none inhibited clathrin-mediated endocytosis (Figure 3B). Chlorpromazine, a known inhibitor of clathrin-mediated endocytosis (Subtil *et al.*, 1994), blocked ~90% of FITC-transferrin uptake, thus validating the assay. Only terfenadine was found to moderately (~10%) inhibit caveolin-mediated endocytosis (Figure 3C). In these experiments, the caveolin-mediated endocytosis inhibitor nystatin was used as a positive control (Zhu *et al.*, 2011). Next, we tested the effect of identified macropinocytosis inhibitors on phagocytosis using the CytoSelect™ Phagocytosis Assay (Cell Biolabs), which utilizes enzyme-labelled *E. coli* particles as a phagocytosis pathogen. Cytochalasin D, a known inhibitor of actin polymerization and phagocytosis (Ting-Beall *et al.*, 1995), was used as a positive control. Our results demonstrated that three of six drugs (auranofin, itraconazole and terfenadine) inhibited phagocytosis by greater than or equal to 20% (Figure 3D). The relatively high inhibitory rate (50%) can be explained by the fact that both macropinocytosis and phagocytosis use the cytoskeleton to extend membrane protrusions and they share several regulatory signalling molecules (Mercer and Helenius, 2009). Taken together, the secondary toxicity and specificity screens identified three macropinocytosis inhibitors (imipramine, phenoxybenzamine and vinblastine) that exert no cytotoxic effects at  $\text{IC}_{100}$  concentrations after a longer exposure and lack inhibitory activities against phagocytosis and clathrin-mediated and caveolin-mediated endocytosis. The microtubule inhibitor vinblastine was removed from further analysis as it inhibits important physiological processes, such as cell cycle, and has serious undesired side effects *in vivo* (Cariou *et al.*, 2010).

### Imipramine inhibits plasma membrane ruffle formation, a critical early step in macropinocytosis

Plasma membrane activities during macropinocytosis can be divided into four consecutive steps: (i) membrane ruffling, (ii) cup formation, (iii) cup closure and (iv) macropinosome

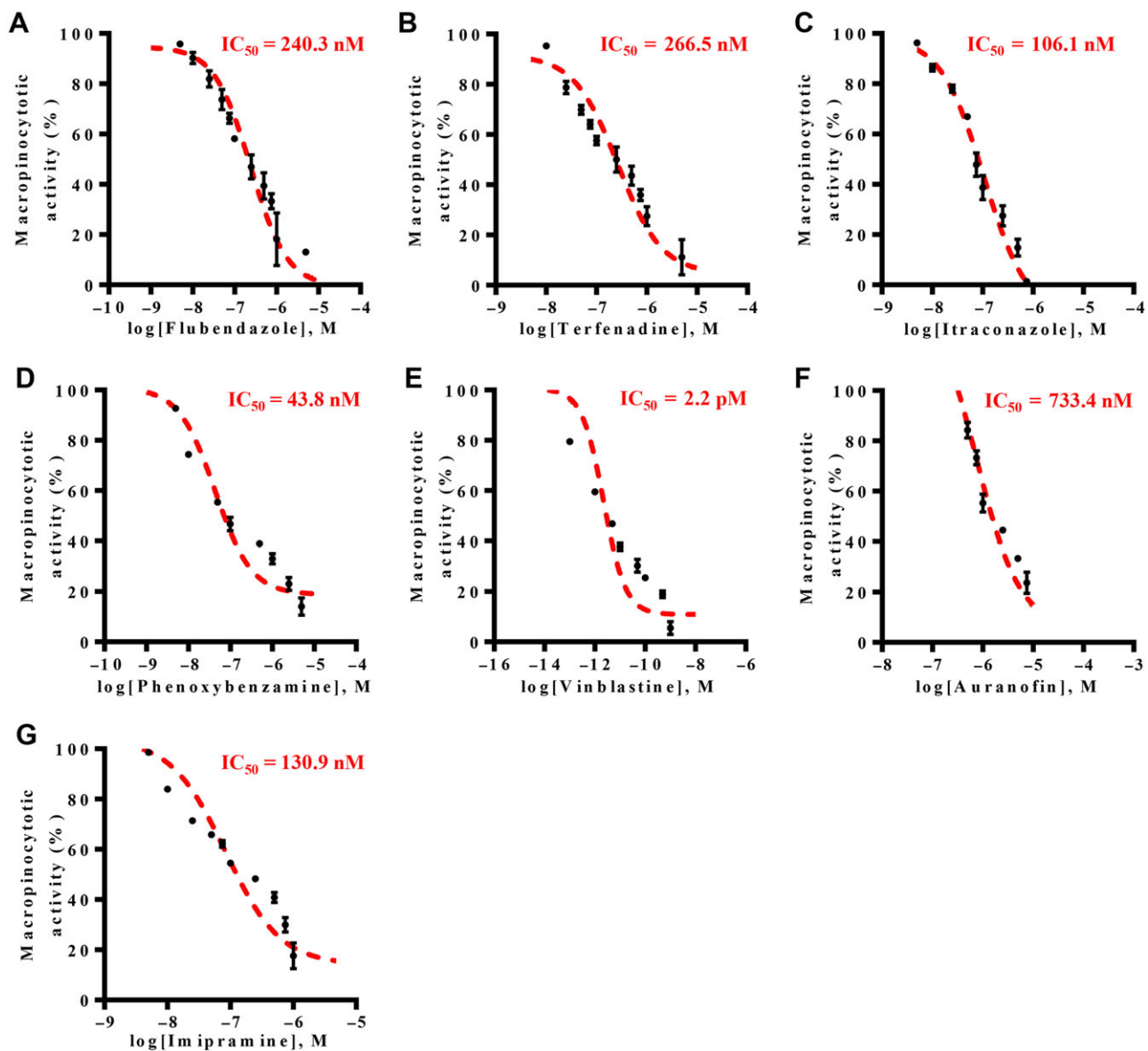


**Figure 2**

$IC_{50}$  values of macropinocytosis inhibitors. Inhibitory concentration curves from which  $IC_{50}$  values for (A) flubendazole, (B) terfenadine, (C) itraconazole, (D) phenoxybenzamine, (E) vinblastine, (F) auranofin and (G) imipramine are presented.  $IC_{50}$  values were estimated from the inhibitor concentrations versus percentage of inhibitory activity relative to the uninhibited control using Prism software. Error bars represent the SD of five independent experiments performed in triplicates.

formation/solute internalization. We next used scanning electron microscopy and confocal imaging to investigate which morphological steps were inhibited by imipramine and phenoxybenzamine. The scanning electron microscopy images demonstrated that PMA stimulated membrane ruffling (yellow arrow), ruffle circularization (red arrow) and cup formation (blue arrow) on the dorsal surface of macrophages (Figure 4A). Pre-incubation of macrophages with phenoxybenzamine partially (65%) inhibited, while imipramine completely blocked PMA-induced membrane ruffle formation (Figure 4B). Interestingly, the remaining ruffles on the surface of phenoxybenzamine-treated macrophages were able to circularize and form cups (Figure 4A), suggesting that

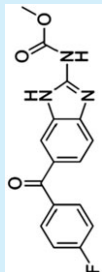
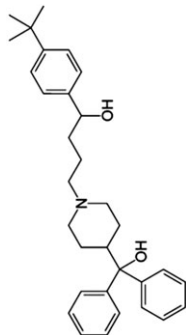
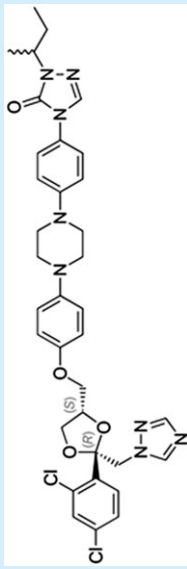
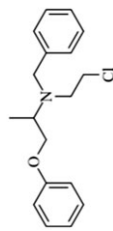
signalling mediators involved in cup closure and/or macropinosome formation are also inhibited by phenoxybenzamine. Inhibition of PMA-induced membrane ruffling by imipramine was confirmed by confocal laser scanning microscopy (Figure 4C).

### *Imipramine did not inhibit $Na^+/H^+$ exchanger activity*

The NHE blocker EIPA is currently considered as the most effective and selective pharmacological tool to inhibit macropinocytosis (Ivanov, 2008; Commisso *et al.*, 2013). As NHE is involved in volume and pH regulation and known to

Table 1

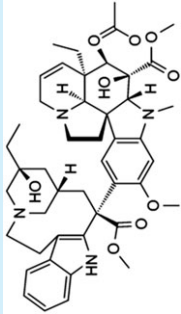
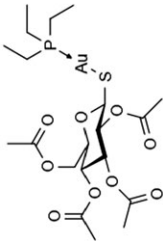
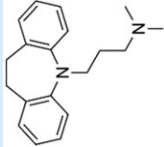
IC<sub>50</sub>, CC<sub>50</sub>, selectivity index and IC<sub>100</sub> values of identified macropinocytosis inhibitors

Drugs	Class	Formula (MW)	Structure	IC <sub>50</sub>	CC <sub>50</sub>	Selectivity index	IC <sub>100</sub>
Flubendazole	Anthelmintic	C <sub>16</sub> H <sub>12</sub> FN <sub>3</sub> O <sub>3</sub> (313.28)		240 ± 33.8 nM	3.4 ± 0.8 μM	14.2	9 μM
Terfenadine	Histamine H <sub>1</sub> -receptor antagonist	C <sub>32</sub> H <sub>41</sub> NO <sub>2</sub> (471.67)		267 ± 49.1 nM	80.1 ± 13.2 μM	301	5 μM
Itraconazole	Antifungal medicine	C <sub>35</sub> H <sub>38</sub> Cl <sub>2</sub> N <sub>8</sub> O <sub>4</sub> (705.64)		106 ± 10.3 nM	7.8 ± 2.0 μM	73.5	1 μM
Phenoxybenzamine	α-Adrenergic antagonist	C <sub>18</sub> H <sub>22</sub> ClNO (303.83)		43.8 ± 10.5 nM	30.2 ± 6.7 μM	6905	5 μM

*continues*



**Table 1**  
(Continued)

Drugs	Class	Formula (MW)	Structure	IC <sub>50</sub>	CC <sub>50</sub>	Selectivity index	IC <sub>100</sub>
Vinblastine	Microtubule formation inhibitor	C <sub>46</sub> H <sub>58</sub> N <sub>4</sub> O <sub>9</sub> (810.98)		2.2 ± 0.7 pM	7.3 ± 0.4 nM	3650	2 nM
Auranofin	Anti-rheumatoid arthritis agent	C <sub>20</sub> H <sub>35</sub> AuO <sub>9</sub> PS <sup>+</sup> (679.49)		733 ± 191 nM	43.7 ± 8.6 μM	59.6	9 μM
Imipramine	TCA	C <sub>19</sub> H <sub>24</sub> N <sub>2</sub> (280.41)		131 ± 26.3 nM	39.4 ± 5.5 μM	301	5 μM

Selectivity index = CC<sub>50</sub>/IC<sub>50</sub>. IC<sub>100</sub>, maximal inhibitory concentration; CC<sub>50</sub>, the 50% cytotoxic concentration.

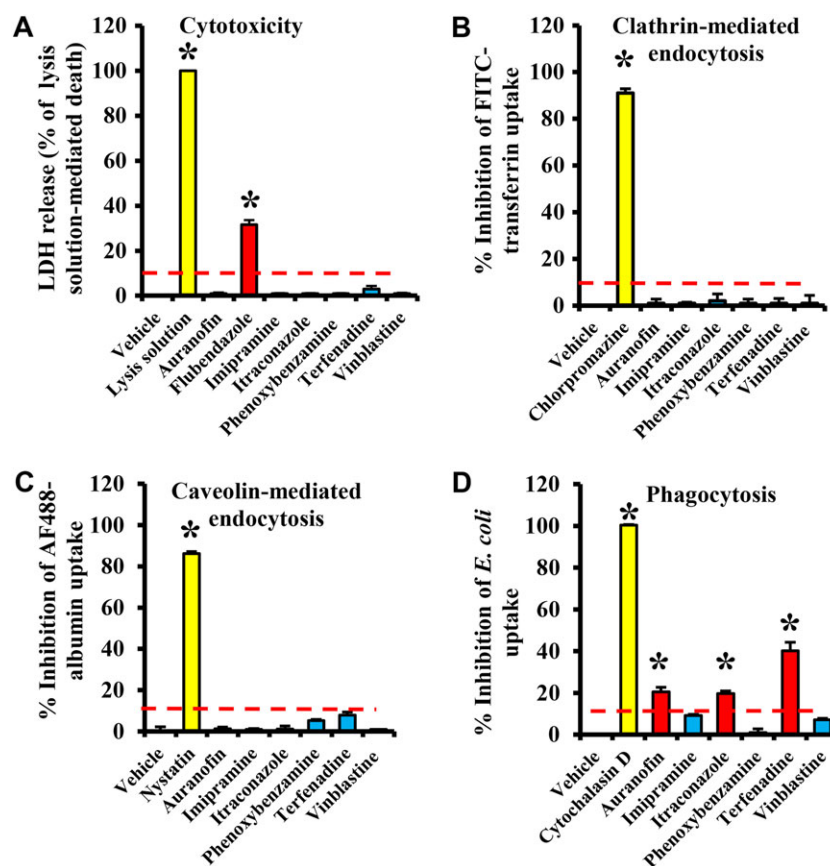


**Figure 3**

Cytotoxicity and selectivity. (A) The effect of identified macropinocytosis inhibitors ( $IC_{100}$ , 24 h) on cell (RAW 264.7 macrophages) viability was determined by a commercially available LDH cytotoxicity kit (Thermo Fisher). Lysis solution-treated cells were used as positive controls. Data are expressed as % of lysis solution-induced LDH release compared with vehicle control. Data represent the mean  $\pm$  SEM.  $n = 5$ ; \* $P < 0.05$ , significantly different from vehicle-treated control by one-way ANOVA with Bonferroni *post hoc* test. Inhibitory effect of identified macropinocytosis inhibitors ( $IC_{100}$ , 60 min) on (B) clathrin-mediated and (C) caveolin-mediated endocytosis. FITC-transferrin ( $1 \mu\text{g}\cdot\text{mL}^{-1}$ ) and AF488-albumin ( $1 \mu\text{g}\cdot\text{mL}^{-1}$ ) were used to investigate clathrin-mediated and caveolin-mediated endocytosis respectively. Chlorpromazine (clathrin,  $10 \mu\text{M}$ , 1 h) and nystatin (caveolin,  $10 \mu\text{M}$ , 1 h) were used as positive controls. Data represent the mean  $\pm$  SEM.  $n = 5$ ; \* $P < 0.05$ , significantly different from vehicle by one-way ANOVA with Bonferroni *post hoc* test. (D) The inhibitory effect of identified macropinocytosis inhibitors on phagocytosis was determined using the CytoSelect™ Phagocytosis Assay (Cell Biolabs). RAW 264.7 macrophages were treated with vehicle, cytochalasin D (positive control) or macropinocytosis inhibitors ( $IC_{100}$ ) for 60 min. Data are presented as % of cytochalasin D-mediated inhibition of *E. coli* phagocytosis. Data represent the mean  $\pm$  SEM.  $n = 5$ ; \* $P < 0.05$ , significantly different from vehicle by one-way ANOVA with Bonferroni *post hoc* test.

regulate the activity of pH sensitive signalling molecules (Pedersen *et al.*, 2007; Hisamitsu *et al.*, 2012), we next investigated whether imipramine inhibits NHE activity. Intracellular pH ( $pH_i$ ) and the functional activity of NHE in macrophages were determined using the ratiometric pH-sensitive dye, BCECF-AM (Swanson *et al.*, 1998). As shown in Figure 5A–C, the rate of  $pH_i$  recovery from an acid load ( $dpH_i/dt$ ) was identical in vehicle-treated and imipramine-treated macrophages. On the other hand, EIPA inhibited the rate of  $pH_i$  recovery, demonstrating the role of NHE in pH regulation (Figure 5B, C). These results suggest that imipramine does not inhibit NHE activity or regulate  $pH_i$  in macrophages.

### Imipramine inhibited ROS signalling but not Ras/MEK/ERK, PKC $\delta$ or PI3K activation

Previous studies demonstrated that increased **Ras** activity stimulates macropinocytosis in both mammalian cells and

*Dictyostelium* (Lim *et al.*, 2002; Palm *et al.*, 2015) and knock-down of Ras leads to an attenuation of macropinocytosis (Commisso *et al.*, 2013). We therefore investigated the effect of imipramine on the activation of downstream Ras effectors MAPK kinase (MEK) and **ERK** using Western blotting. PMA treatment rapidly (5 min) stimulated MEK and ERK phosphorylation in macrophages (Figure 6A–C). Pretreatment of macrophages with imipramine did not inhibit PMA-induced phosphorylation of MEK and ERK, suggesting that inhibition of Ras/MEK/ERK signalling is not responsible for the inhibitory effect of imipramine on macropinocytosis.

**PKC** activation plays a critical role in macropinocytosis (Singla *et al.*, 2018). To investigate whether imipramine inhibits PKC activation in macrophages, we measured the phosphorylation status of PKC $\delta$  (major PKC isoform in macrophages) following PMA,  $\pm$ imipramine treatment. Our results demonstrated that imipramine does not inhibit PMA-induced activation of PKC $\delta$  (Figure 6A, D).

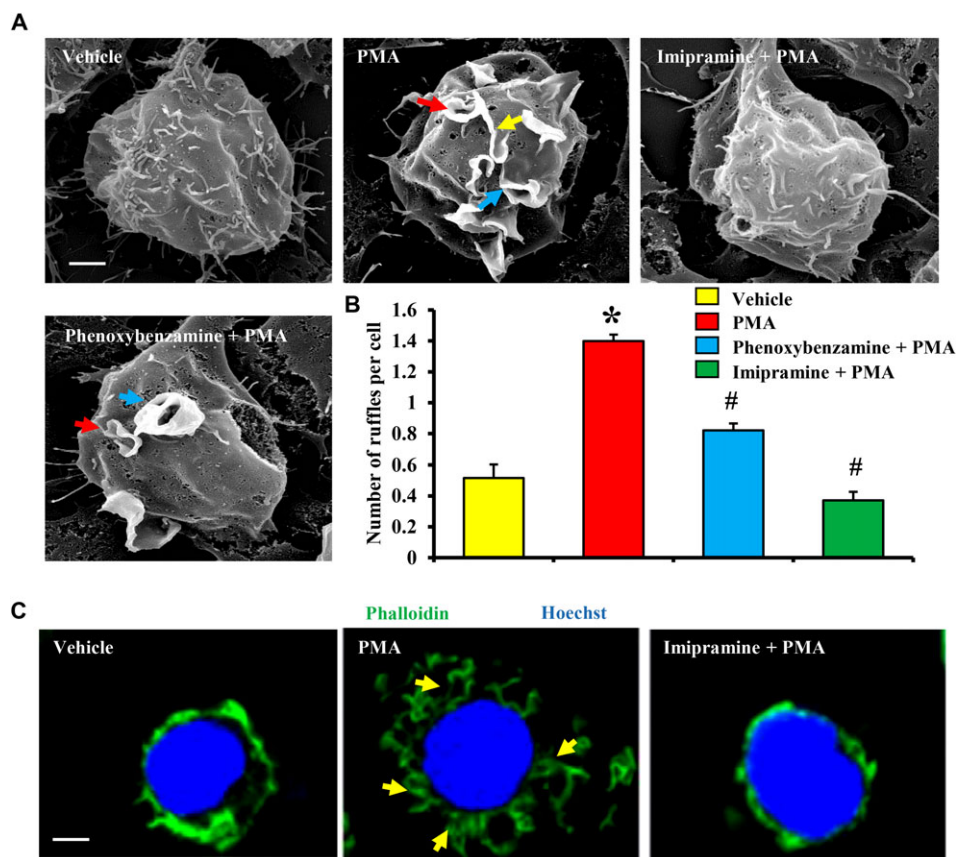


**Figure 4**

Imipramine inhibits membrane ruffle formation. (A) RAW 264.7 macrophages were treated with vehicle, PMA (1  $\mu$ M, 30 min) or pretreated with imipramine (5  $\mu$ M, 60 min) or phenoxybenzamine (5  $\mu$ M, 60 min) and then challenged with PMA. Cells were processed for SEM imaging. Membrane ruffles (yellow arrows), circularized C-shaped ruffles (red arrows) and macropinocytotic cups (blue arrows) were observed on the dorsal surface of PMA-treated macrophages. Circularized ruffles and macropinocytotic cups were also observed on some phenoxybenzamine + PMA-treated cells. Scale bar: 2  $\mu$ m. (B) Bar graph shows quantification of membrane ruffles normalized to total cell number. Data represent the mean  $\pm$  SEM.  $n = 5$ ; \* $P < 0.05$ , significantly different from vehicle, # $P < 0.05$ , significantly different from PMA by one-way ANOVA with Bonferroni *post hoc* test. (C) Macrophages were treated with vehicle, PMA or imipramine + PMA as described in (A) and fixed in 2% PFA. Nuclei were stained by Hoechst (blue) and F-actin was labelled by 488 phalloidin (green). Yellow arrows indicate membrane ruffle formation in PMA-treated cells. Images were taken with a Zeiss 780 confocal microscope (63 $\times$ ; scale bar: 5  $\mu$ m). Similar results have been observed in six independent experiments.

Pharmacological inhibitors of PI3K (i.e. wortmannin) inhibit macropinocytosis (Palm *et al.*, 2017). We next investigated whether imipramine inhibits PMA-induced PI3K activity in macrophages using a PI3K activity ELISA kit (Echelon Biosciences). Our results indicated that imipramine does not inhibit PI3K activity (Figure 6E).

Our laboratory has recently demonstrated that **NADPH oxidase 2 (Nox2)**-derived ROS mediate initiation of membrane ruffle formation in response to PMA and M-CSF treatments (Ghoshal *et al.*, 2017). As shown in Figure 6F, G, pretreatment of macrophages partially (50%) inhibited PMA-induced ROS formation in macrophages. The specificity of L-012 for superoxide anion ( $O_2^{\cdot -}$ ) was confirmed by the addition of SOD (150 U·mL $^{-1}$ ). These data suggest that imipramine may inhibit macropinocytosis through inhibition of redox signalling. Further studies are required to identify the precise mechanism(s) by which imipramine inhibits macropinocytosis.

### *Imipramine inhibited macropinocytosis in cancer cells, dendritic cells and macrophages*

Macropinocytosis has been implicated in a variety of pathological conditions, including cancer (Lim and Gleeson, 2011), allergic disorders (Sallusto *et al.*, 1995) and atherosclerosis (Kruth *et al.*, 2005). Cancer cells support their increased metabolic needs by nutrient macropinocytosis, which in turn leads to their increased proliferation *in vitro* and tumour growth *in vivo* (Commisso *et al.*, 2013). As shown in Figure 7A, pre-incubation of 4T1 mammary carcinoma cells with imipramine inhibited PMA-induced macropinocytosis. Immature dendritic cells internalize antigens *via* macropinocytosis and present the processed antigenic peptides to T-cells to initiate an adaptive immune response (Sallusto *et al.*, 1995). Our FACS results demonstrated that PMA-induced antigen (ovalbumin) macropinocytosis was inhibited in CD11c $^+$  immature dendritic cells (Figure 7B). Also, macrophages internalize unmodified, native LDL

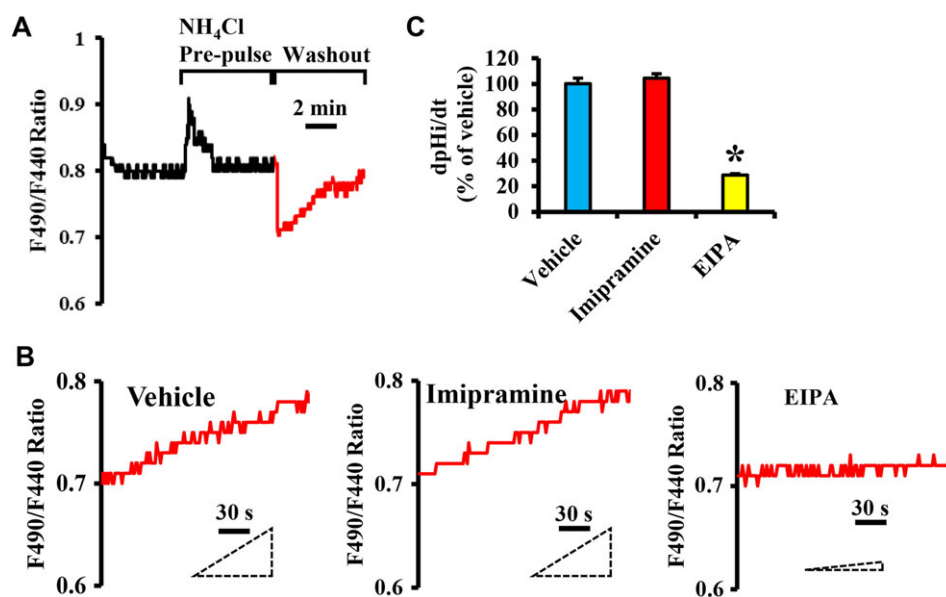


**Figure 5**

Imipramine does not inhibit NHE activity in macrophages. (A) Representative tracing showing changes in intracellular pH ( $pH_i$ ) (F490/F440 ratio) following treatment with  $NH_4Cl$  (20 mM) and during washout period. The rate of  $pH_i$  recovery ( $dpH_i/dt$ ) from the acid load is an index of NHE activity (red tracing). (B) Representative  $pH_i$  recovery tracings in RAW 264.7 macrophages from the acid load following treatment with vehicle, imipramine (5  $\mu M$ , 60 min) and EIPA (25  $\mu M$ , 60 min). (C) Bar graphs show quantified  $dpH_i/dt$  changes in macrophages during the recovery phase. Data are expressed as % of vehicle-induced changes in  $dpH_i/dt$ . Data represent the mean  $\pm$  SEM.  $n = 5$ ; \* $P < 0.05$ , significantly different from vehicle by one-way ANOVA with Bonferroni *post hoc* test.

(nLDL) *via* macropinocytosis, leading to significant cholesterol accumulation and foam cell formation (Kruth *et al.*, 2002). Importantly, this process may contribute to atherosclerosis, independent of the classical scavenger receptor-mediated lipid internalization pathways (Csanyi *et al.*, 2017). As shown in Figure 7C, pre-incubation of macrophages with imipramine inhibited PMA-induced intracellular lipid accumulation in macrophages following nLDL treatment. In summary, these results demonstrate that imipramine inhibits stimulated macropinocytosis in a range of different cell types and suggest its potential as a new pharmacological tool to elucidate more fully the role of macropinocytosis in pathological processes.

## Discussion

Macropinocytosis is a highly conserved, actin-dependent endocytic process by which extracellular fluid and pericellular solutes are internalized into cells. In the past few years, evidence has been accumulating that increased rate of macropinocytosis contributes to various pathological processes, including cardiovascular disorders, cancer, allergic diseases, Alzheimer's disease and bacterial/viral infections (Kruth *et al.*, 2005; Mercer and Helenius, 2009; Comisso *et al.*, 2013; Tang *et al.*, 2015). Unfortunately, most currently available inhibitors of macropinocytosis have limited bioavailability (Smith and Smith, 1973), inhibit other endocytic processes and have non-specific endocytosis-independent effects (Ivanov, 2008). Although in recent years pharmacological inhibition of macropinocytosis has

emerged as a promising concept for the treatment of various diseases, no efforts have been made prior to this study to identify macropinocytosis inhibitors suitable for clinical use.

Interestingly, a recent study using the Molecular Libraries Small Molecule Repository library identified two chemical compounds that inhibit virus-induced macropinocytosis (Anantpadma *et al.*, 2016). The ability of these compounds to inhibit phagocytosis or caveolin-mediated endocytosis and their pharmacological/safety profiles were not investigated. In the present study, we have utilized a commercially available library with compounds that are already used in the clinic for treatment of various diseases to identify low MW compounds that inhibit macropinocytosis. The advantage of such a screen is that the drugs have been already tested in humans (and animals) and the concentrations at which the drugs are toxic, their pharmacological profile and potential side effects are known. As such, these compounds are ideal candidates for *in vitro* and *in vivo* basic research use as well as drug repurposing. The primary screen identified 14 compounds that at  $\sim 10$   $\mu M$  inhibited  $>95\%$  of macropinocytotic solute internalization in macrophages. A series of secondary screens confirmed the inhibitory activity for nine of these 14 drugs that blocked both PMA-induced and M-CSF (physiological stimulator)-induced macropinocytosis in RAW cells. Of these hits, two compounds were eliminated due to their incomplete ( $\sim 50\%$ ) inhibition of macropinocytosis in primary murine macrophages. In these experiments, inhibitory activities of identified compounds ( $\sim 10$   $\mu M$ ) were comparable to that of EIPA (25  $\mu M$ ) though at slightly lower concentrations.  $IC_{50}$  values of identified inhibitors were in the 40–700 nM range, with the



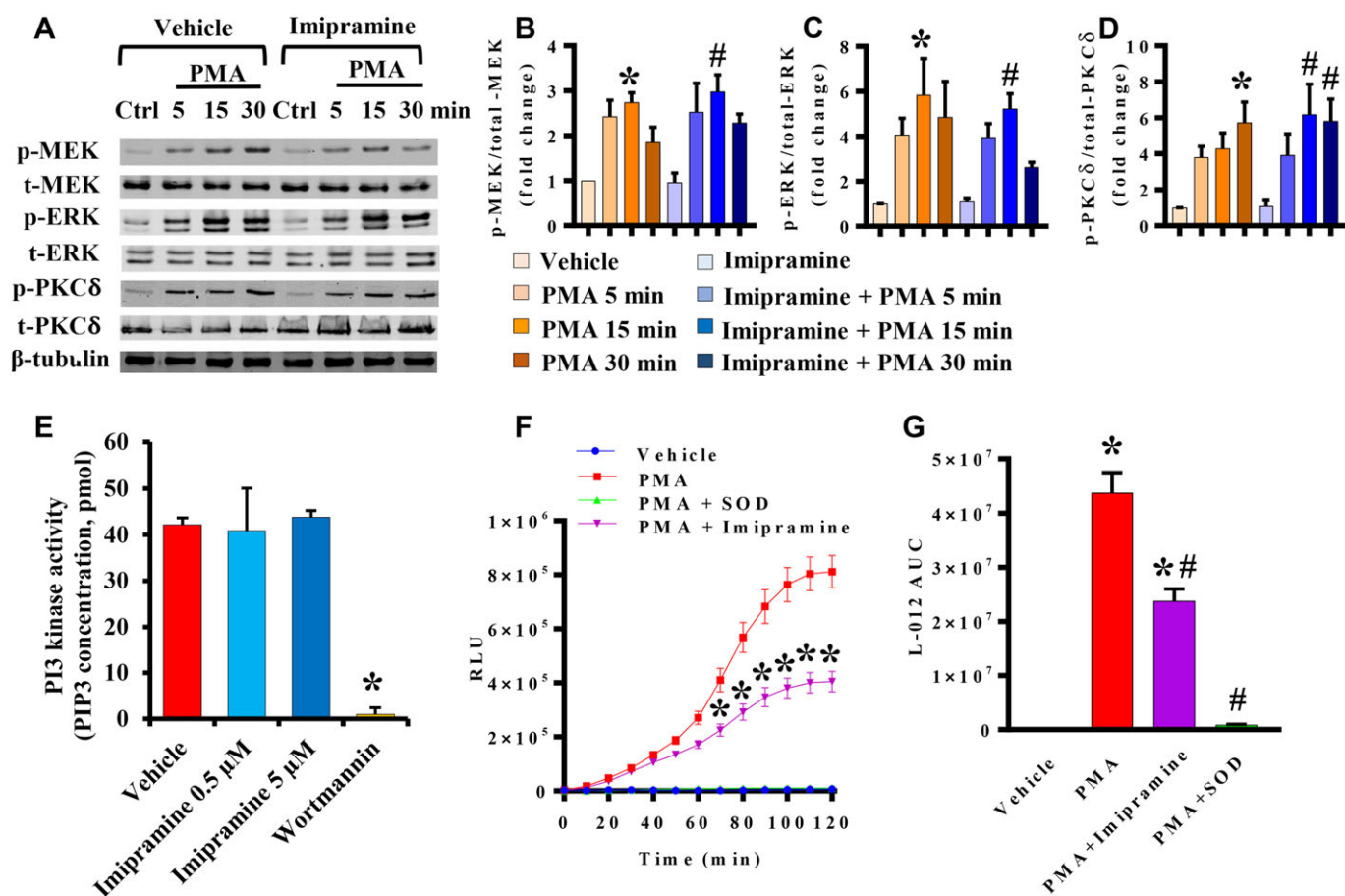


**Figure 6**

Imipramine inhibits ROS signalling but not Ras/MEK/ERK, PKCδ or PI3K activation in macrophages. (A) Representative Western blot images for p-MEK, t-MEK, p-ERK, t-ERK, p-PKCδ, t-PKCδ and β-tubulin are shown. (B–D) Bar graphs represent averaged OD data expressed as a ratio of phosphoproteins to total proteins  $n = 5$ ; \* $P < 0.05$ , significantly different from vehicle, # $P < 0.05$ , significantly different from imipramine. (E) PI3K activity (PIP3 production) was analysed using ELISA.  $n = 5$ , \* $P < 0.05$ , significantly different from vehicle. (F) O<sub>2</sub><sup>-</sup> generation in RAW 264.7 macrophages using L-012 chemiluminescence.  $n = 5$ , \* $P < 0.05$  versus PMA by one-way ANOVA with Bonferroni *post hoc* test at each time point. (G) The diagram represents the L-012 chemiluminescence AUC.  $n = 5$ . \* $P < 0.05$ , significantly different from vehicle, # $P < 0.05$ , significantly different from PMA by one-way ANOVA with Bonferroni *post hoc* test.

exception of vinblastine, which was effective at low pM concentrations. Thus, a total of seven drugs, namely, auranofin, flubendazole, imipramine, itraconazole, phenoxybenzamine, terfenadine and vinblastine, proceeded to the cytotoxicity and selectivity testing. Flubendazole was found to be cytotoxic after longer exposure times and eliminated. The remaining six compounds had no inhibitory activity against clathrin-mediated and caveolin-mediated endocytosis. Auranofin, itraconazole and terfenadine, on the other hand, inhibited phagocytosis. These three drugs, therefore, were excluded from further analysis. The microtubule inhibitor vinblastine was also excluded from further study as it is known to inhibit the cell cycle at low concentrations and have serious undesired side effects *in vivo* (Cariou *et al.*, 2010). Interestingly, the inhibitory effect of vinblastine on macropinocytosis supports the role of microtubule-mediated intracellular transport (i.e. cytosol to membrane) in macropinocytosis. Moreover, these findings raise the question whether the anti-cancer effect of vinblastine is also mediated, at least partially, through inhibition of

macropinocytosis. In summary, the primary and secondary screens identified two compounds (imipramine and phenoxybenzamine) that inhibited macropinocytosis without exerting cytotoxic effects or inhibiting phagocytosis and clathrin-mediated and caveolin-mediated endocytosis.

Next, we used scanning electron microscopy and confocal imaging to investigate which morphological step during macropinocytosis was inhibited by imipramine and phenoxybenzamine. Our results indicated that pre-incubation of macrophages with imipramine inhibits phorbol ester-stimulated membrane ruffle formation. Interestingly, only partial inhibition of membrane ruffling was observed following treatment with phenoxybenzamine, with the remaining ruffles capable of circularizing and forming cups. These results suggest that imipramine inhibits activation of signalling molecules involved in membrane ruffling, while phenoxybenzamine inhibits multiple signalling pathways mediating both early ruffle formation and plasma membrane activities downstream of cup formation (i.e. cup closure and/or macropinosome formation).

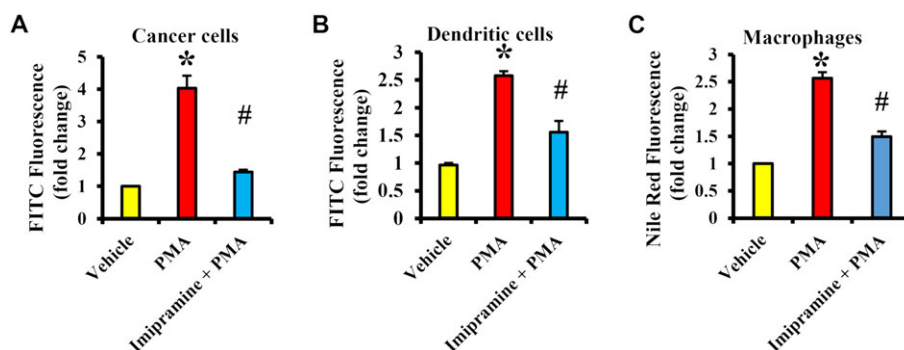


**Figure 7**

Imipramine inhibits macropinocytosis in cancer cells, immature dendritic cells and macrophages. (A) 4T1 cells were pretreated with vehicle or imipramine (5  $\mu$ M) for 60 min and stimulated with PMA (1  $\mu$ M, 2 h) in the presence of FITC-dextran. FITC fluorescence was determined by FACS analysis;  $n = 5$ . (B) Bone-marrow derived immature dendritic cells were characterized by high-level expression of CD11c (CD11c<sup>+</sup>), low-level to intermediate-level expression of MHC II and low-level expression of CD86 (not shown). LPS from *E. coli*, a known dendritic cell maturation agent, was used as a positive control to determine the maturation status of dendritic cells. CD11c<sup>+</sup> immature dendritic cells were treated as described in (A) and incubated with FITC-ovalbumin. FITC fluorescence was determined by FACS analysis;  $n = 5$ . (C) RAW 264.7 macrophages were treated with nLDL (50  $\mu$ g·mL<sup>-1</sup>) and incubated with vehicle, PMA or imipramine + PMA for 24 h. Cells were fixed in 2% PFA, internalized lipids stained by Nile Red and FACS analysis performed,  $n = 5$ . Data are presented as fold change of vehicle treatment to control for variation between independent experiments. Data represent the mean  $\pm$  SEM. \* $P < 0.05$ , significantly different from vehicle; # $P < 0.05$ , significantly different from PMA by one-way ANOVA with Bonferroni *post hoc* test.

The goal of the next experiments was to identify the possible mechanisms by which imipramine inhibits macropinocytosis. Mechanistically, we found that imipramine does not inhibit activation of Ras/MEK/ERK, PKC $\delta$  and PI3K in macrophages. On the other hand, chemiluminescence O<sub>2</sub><sup>-</sup> detection experiments demonstrated that imipramine inhibits PMA-induced O<sub>2</sub><sup>-</sup> production in macrophages. Previous studies by our lab demonstrated that PMA, M-CSF and HGF stimulate macropinocytosis *via* Nox2 activation and induction of downstream redox signalling (Ghoshal *et al.*, 2017; Singla *et al.*, 2018). Based on these results, we propose that imipramine directly inhibits Nox2 activation (major source of O<sub>2</sub><sup>-</sup> in macrophages) or acts as an antioxidant. It is, however, unknown whether a partial (50%) inhibition of O<sub>2</sub><sup>-</sup> levels is sufficient to inhibit macropinocytosis. At present, the mechanism(s) by which imipramine inhibits macropinocytosis is unknown and requires further investigation.

Pharmacological inhibition of NHE represents the most widely used and accepted method to investigate the role of macropinocytosis in endocytic processes *in vitro* as well as in the pathogenesis of disease development *in vivo* (Ivanov, 2008; Commisso *et al.*, 2013). As NHEs are ubiquitously expressed transmembrane proteins that regulate intracellular sodium concentration, cellular and body water homeostasis and potentially all pH sensitive signalling pathways, results especially from *in vivo* studies employing NHE blockers would require confirmation using alternative, more specific approaches. Importantly, our experiments demonstrated that imipramine does not inhibit NHE or regulate intracellular pH in macrophages. Other advantages of imipramine compared with currently used macropinocytosis inhibitors are its excellent bioavailability following p.o. administration (95%) and its relatively long biological half-life (~20 h) (Heck *et al.*, 1979). Introduced into medicine in the 1960s, imipramine was the first tricyclic antidepressant (TCA), a class named for its three-ring molecular structure. Imipramine

inhibits reuptake of the neurotransmitters **noradrenaline** and **5-HT** in the brain and blocks **muscarinic cholinergic** and **dopamine receptors** (Tatsumi *et al.*, 1997). These mechanisms must be considered when imipramine is used as a macropinocytosis inhibitor especially in *in vivo* experiments. With this said, we anticipate that structure–activity relationship studies using TCAs may yield novel compounds that maintain their inhibitory effect on macropinocytosis but exert no effect on neurotransmitter uptake or inhibit dopaminergic and muscarinic receptors. This is currently an area of active investigation in our laboratory. Taking this even further, an exciting area of research would be the conjugation of selective macropinocytosis inhibitors with ‘homing’ peptides to achieve tissue-specific inhibition of macropinocytosis (Ye and Yang, 2009). Relevant to this, we showed that imipramine inhibits stimulated macropinocytosis in several cell types, including cancer cells, dendritic cells and macrophages. Finally, an ideal macropinocytosis inhibitor would block only stimulated macropinocytosis as constitutive macropinocytosis is involved in the regulation of physiological processes (Sallusto *et al.*, 1995; Liu and Roche, 2015). Importantly, our scanning electron microscopy data on the quantification of the membrane ruffles suggest that imipramine does not inhibit constitutive membrane ruffling in macrophages.

In summary, we report here the development of a systematic screen designed to identify low MW inhibitors of macropinocytosis. By screening a library of 640 FDA-approved compounds, the primary screen and subsequent secondary analyses identified a low MW drug, imipramine, that blocked membrane ruffle formation and inhibited macropinocytosis in macrophages, dendritic cells and cancer cells. We anticipate that the identified macropinocytosis inhibitor will prove useful as a pharmacological tool to more fully explore the role of macropinocytosis in pathological processes. Our study also suggests that imipramine and

potentially other TCAs might be good candidates for repurposing as therapeutic agents in pathological processes involving macropinocytosis and serve as a chemical platform for developing more specific inhibitors of macropinocytosis.

## Acknowledgements

The authors wish to thank Jeanene Pihkala and Libby Perry (Augusta University) for their help with the FACS analysis and sample preparation for the scanning electron microscopy experiments, respectively. The authors are grateful to Dr Thomas Albers (Augusta University) for his valuable suggestions and guidance on the experimental results. This work was supported by National Institutes of Health grants (K99HL114648 and R00HL114648) awarded to Gabor Csanyi and American Heart Association Postdoctoral Fellowship (17POST33661254) given to Bhupesh Singla.

## Author contributions

G.C., H.-P.L., B.S. and P.G. contributed in the conception or design of the work; H.-P.L., B.S., P.G., M.C.-S., J.L.F., E.J.B.D. C., P.M.O. and G.C. in the acquisition of the data, data collection and data analysis; H.-P.L. and G.C. in the writing and reviewing of the manuscript; J.-X.S. provided the FDA-approved drug library; and all authors approved the final version of the manuscript and agreed to be accountable for all aspects of the work in ensuring that questions related to the accuracy or integrity of any part of the work are appropriately investigated and resolved.

## Conflict of interest

The authors declare no conflicts of interest.

## Declaration of transparency and scientific rigour

This Declaration acknowledges that this paper adheres to the principles for transparent reporting and scientific rigour of preclinical research recommended by funding agencies, publishers and other organisations engaged with supporting research.

## References

- Aleksandrowicz P, Marzi A, Biedenkopf N, Beimforde N, Becker S, Hoenen T *et al.* (2011). Ebola virus enters host cells by macropinocytosis and clathrin-mediated endocytosis. *J Infect Dis* 204 (Suppl 3): S957–S967.
- Alexander SPH, Kelly E, Marrion NV, Peters JA, Faccenda E, Harding SD *et al.* (2017a). The Concise Guide to PHARMACOLOGY 2017/18: Other proteins. *Br J Pharmacol* 174: S1–S16.
- Alexander SPH, Kelly E, Marrion NV, Peters JA, Faccenda E, Harding SD *et al.* (2017b). The Concise Guide to PHARMACOLOGY 2017/18: Transporters. *Br J Pharmacol* 174: S360–S446.
- Alexander SPH, Fabbro D, Kelly E, Marrion NV, Peters JA, Faccenda E *et al.* (2017c). The Concise Guide to PHARMACOLOGY 2017/18: Enzymes. *Br J Pharmacol* 174: S272–S359.
- Alexander SPH, Peters JA, Kelly E, Marrion NV, Faccenda E, Harding SD *et al.* (2017d). The Concise Guide to PHARMACOLOGY 2017/18: Ligand-gated ion channels. *Br J Pharmacol* 174: S130–S159.
- Alexander SPH, Christopoulos A, Davenport AP, Kelly E, Marrion NV, Peters JA *et al.* (2017e). The Concise Guide to PHARMACOLOGY 2017/18: G protein-coupled receptors. *Br J Pharmacol* 174 (Suppl 1): S17–S129.
- Anantpadma M, Kouznetsova J, Wang H, Huang R, Kolokoltsov A, Guha R *et al.* (2016). Large-scale screening and identification of novel Ebola virus and Marburg virus entry inhibitors. *Antimicrob Agents Chemother* 60: 4471–4481.
- Araki N, Johnson MT, Swanson JA (1996). A role for phosphoinositide 3-kinase in the completion of macropinocytosis and phagocytosis by macrophages. *J Cell Biol* 135: 1249–1260.
- Ashburn TT, Thor KB (2004). Drug repositioning: identifying and developing new uses for existing drugs. *Nat Rev Drug Discov* 3: 673–683.
- Berry R, Call ME (2017). Modular activating receptors in innate and adaptive immunity. *Biochemistry* 56: 1383–1402.
- Bohdanowicz M, Grinstein S (2013). Role of phospholipids in endocytosis, phagocytosis, and macropinocytosis. *Physiol Rev* 93: 69–106.
- Botelho RJ, Teruel M, Dierckman R, Anderson R, Wells A, York JD *et al.* (2010). Localized biphasic changes in phosphatidylinositol-4,5-bisphosphate at sites of phagocytosis. *J Cell Biol* 151: 1353–1368.
- Cariou O, Laroche-Prigent N, Ledieu S, Guizon I, Paillard F, Thybaud V (2010). Cytosine arabinoside, vinblastine, 5-fluorouracil and 2-aminoanthracene testing in the *in vitro* micronucleus assay with L5178Y mouse lymphoma cells at Sanofi Aventis, with different cytotoxicity measurements, in support of the draft OECD Test Guideline on *In Vitro* Mammalian Cell Micronucleus Test. *Mutat Res* 702: 148–156.
- Chung JJ, Huber TB, Godel M, Jarad G, Hartleben B, Kwok C *et al.* (2015). Albumin-associated free fatty acids induce macropinocytosis in podocytes. *J Clin Invest* 125: 2307–2316.
- Commisso C, Davidson SM, Soydaner-Azeloglu RG, Parker SJ, Kamphorst JJ, Hackett S *et al.* (2013). Macropinocytosis of protein is an amino acid supply route in Ras-transformed cells. *Nature* 497: 633–637.
- Csanyi G, Feck DM, Ghoshal P, Singla B, Lin H, Nagarajan S *et al.* (2017). CD47 and Nox1 mediate dynamic fluid-phase macropinocytosis of native LDL. *Antioxid Redox Signal* 26: 886–901.
- Csanyi G, Yao M, Rodriguez AI, Al Ghouleh I, Sharifi-Sanjani M, Frazziano G *et al.* (2012). Thrombospondin-1 regulates blood flow via CD47 receptor-mediated activation of NADPH oxidase 1. *Arterioscler Thromb Vasc Biol* 32: 2966–2973.
- Curtis MJ, Alexander S, Cirino G, Docherty JR, George CH, Gienbycz MA *et al.* (2018). Experimental design and analysis and their reporting II: updated and simplified guidance for authors and peer reviewers. *Brit J Pharmacol* 175: 987–993.
- Ghoshal P, Singla B, Lin H, Feck DM, Cantu-Medellin N, Kelley EE *et al.* (2017). Nox2-mediated PI3K and cofilin activation confers alternate redox control of macrophage pinocytosis. *Antioxid Redox Signal* 26: 902–916.

- Grimmer S, Van Deurs B, Sandvig K (2002). Membrane ruffling and macropinocytosis in A431 cells require cholesterol. *J Cell Sci* 115: 2953–2962.
- Harding SD, Sharman JL, Faccenda E, Southan C, Pawson AJ, Ireland S *et al.* (2018). The IUPHAR/BPS Guide to PHARMACOLOGY in 2018: updates and expansion to encompass the new guide to IMMUNOPHARMACOLOGY. *Nucl Acids Res.* 46: D1091–D1106.
- Heck HA, Buttrill SE Jr, Flynn NW, Dyer RL, Anbar M, Cairns T *et al.* (1979). Bioavailability of imipramine tablets relative to a stable isotope-labeled internal standard: increasing the power of bioavailability tests. *J Pharmacokinet Biopharm* 7: 233–248.
- Hisamitsu T, Nakamura TY, Wakabayashi S (2012). Na<sup>+</sup>/H<sup>+</sup> exchanger 1 directly binds to calcineurin A and activates downstream NFAT signaling, leading to cardiomyocyte hypertrophy. *Mol Cell Biol* 32: 3265–3280.
- Ivanov AI (2008). Pharmacological inhibition of endocytic pathways: is it specific enough to be useful? *Methods Mol Biol* 440: 15–33.
- Kanlaya R, Sintiprungrat K, Chaiyarit S, Thongboonkerd V (2013). Macropinocytosis is the major mechanism for endocytosis of calcium oxalate crystals into renal tubular cells. *Cell Biochem Biophys* 67: 1171–1179.
- Kilkenny C, Browne WJ, Cuthill IC, Emerson M, Altman DG (2010). Improving bioscience research reporting: the ARRIVE guidelines for reporting animal research. *J Pharmacol Pharmacother* 1: 94–99.
- Kohn AD, Summers SA, Birnbaum MJ, Roth RA (1996). Expression of a constitutively active Akt Ser/Thr kinase in 3T3-L1 adipocytes stimulates glucose uptake and glucose transporter 4 translocation. *J Biol Chem* 271: 31372–31378.
- Koivusalo M, Welch C, Hayashi H, Scott CC, Kim M, Alexander T *et al.* (2010). Amiloride inhibits macropinocytosis by lowering submembranous pH and preventing Rac1 and Cdc42 signaling. *J Cell Biol* 188: 547–563.
- Kruth HS, Huang W, Ishii I, Zhang WY (2002). Macrophage foam cell formation with native low density lipoprotein. *J Biol Chem* 277: 34573–34580.
- Kruth HS, Jones NL, Huang W, Zhao B, Ishii I, Chang J *et al.* (2005). Macropinocytosis is the endocytic pathway that mediates macrophage foam cell formation with native low density lipoprotein. *J Biol Chem* 280: 2352–2360.
- Lim CJ, Spiegelman GB, Weeks G (2002). Cytoskeletal regulation by *Dictyostelium* Ras subfamily proteins. *J Muscle Res Cell Motil* 23: 729–736.
- Lim JP, Gleeson PA (2011). Macropinocytosis: an endocytic pathway for internalising large gulps. *Immunol Cell Biol* 89: 836–843.
- Liu Z, Roche PA (2015). Macropinocytosis in phagocytes: regulation of MHC class-II-restricted antigen presentation in dendritic cells. *Front Physiol* 6: 1.
- McGrath JC, Lilley E (2015). Implementing guidelines on reporting research using animals (ARRIVE etc.): new requirements for publication in BJP. *Br J Pharmacol* 172: 3189–3193.
- Mercer J, Helenius A (2009). Virus entry by macropinocytosis. *Nat Cell Biol* 11: 510–520.
- Nakase I, Kobayashi NB, Takatani-Nakase T, Yoshida T (2015). Active macropinocytosis induction by stimulation of epidermal growth factor receptor and oncogenic Ras expression potentiates cellular uptake efficacy of exosomes. *Sci Rep* 5: 10300.
- Norbury CC (2006). Drinking a lot is good for dendritic cells. *Immunology* 117: 443–451.
- Palm W, Araki J, King B, Dematteo RG, Thompson CB (2017). Critical role for PI3-kinase in regulating the use of proteins as an amino acid source. *Proc Natl Acad Sci U S A* 114: E8628–E8636.
- Palm W, Park Y, Wright K, Pavlova NN, Tuveson DA, Thompson CB (2015). The utilization of extracellular proteins as nutrients is suppressed by mTORC1. *Cell* 162: 259–270.
- Pedersen SF, Darborg BV, Rasmussen M, Nylandsted J, Hoffmann EK (2007). The Na<sup>+</sup>/H<sup>+</sup> exchanger, NHE1, differentially regulates mitogen-activated protein kinase subfamilies after osmotic shrinkage in Ehrlich Lettre Ascites cells. *Cell Physiol Biochem* 20: 735–750.
- Potts BE, Hart ML, Snyder LL, Boyle D, Mosier DA, Chapes SK (2008). Differentiation of C2D macrophage cells after adoptive transfer. *Clin Vaccine Immunol* 15: 243–252.
- Sallusto F, Cella M, Danieli C, Lanzavecchia A (1995). Dendritic cells use macropinocytosis and the mannose receptor to concentrate macromolecules in the major histocompatibility complex class II compartment: downregulation by cytokines and bacterial products. *J Exp Med* 182: 389–400.
- Singla B, Ghoshal P, Lin H, Wei Q, Dong Z, Csanyi G (2018). PKC $\delta$ -mediated Nox2 activation promotes fluid-phase pinocytosis of antigens by immature dendritic cells. *Front Immunol* 9: 537.
- Smith AJ, Smith RN (1973). Kinetics and bioavailability of two formulations of amiloride in man. *Br J Pharmacol* 48: 646–649.
- Stockinger W, Zhang SC, Trivedi V, Jarzylo LA, Shieh EC, Lane WS *et al.* (2006). Differential requirements for actin polymerization, calmodulin, and Ca<sup>2+</sup> define distinct stages of lysosome/phagosome targeting. *Mol Biol Cell* 17: 1697–1710.
- Subtil A, Hemar A, Dautry-Varsat A (1994). Rapid endocytosis of interleukin 2 receptors when clathrin-coated pit endocytosis is inhibited. *J Cell Sci* 107 (Pt 12): 3461–3468.
- Swanson SJ, Bethke PC, Jones RL (1998). Barley aleurone cells contain two types of vacuoles. Characterization of lytic organelles by use of fluorescent probes. *Plant Cell* 10: 685–698.
- Tang W, Tam JH, Seah C, Chiu J, Tyrer A, Cregan SP *et al.* (2015). Arf6 controls  $\beta$ -amyloid production by regulating macropinocytosis of the amyloid precursor protein to lysosomes. *Mol Brain* 8: 41.
- Tatsumi M, Groshan K, Blakely RD, Richelson E (1997). Pharmacological profile of antidepressants and related compounds at human monoamine transporters. *Eur J Pharmacol* 340: 249–258.
- Thomas R, Lipsky PE (1996). Dendritic cells: origin and differentiation. *Stem Cells* 14: 196–206.
- Ting-Beall HP, Lee AS, Hochmuth RM (1995). Effect of cytochalasin D on the mechanical properties and morphology of passive human neutrophils. *Ann Biomed Eng* 23: 666–671.
- Ye X, Yang D (2009). Recent advances in biological strategies for targeted drug delivery. *Cardiovasc Hematol Disord Drug Targets* 9: 206–221.
- Yoshida S, Hoppe AD, Araki N, Swanson JA (2009). Sequential signaling in plasma-membrane domains during macropinosome formation in macrophages. *J Cell Sci* 122: 3250–3261.
- Zhang M, Zhu Q, Shi M, Liu Y, Ma L, Yang Y *et al.* (2015). Active phagocytosis of *Mycobacterium tuberculosis* (H37Ra) by T lymphocytes (Jurkat cells). *Mol Immunol* 66: 429–438.
- Zhu XD, Zhuang Y, Ben JJ, Qian LL, Huang HP, Bai H *et al.* (2011). Caveolae-dependent endocytosis is required for class A macrophage scavenger receptor-mediated apoptosis in macrophages. *J Biol Chem* 286: 8231–8239.